Newly Designed ZVS Multi-Input Converter

Rong-Jong Wai, *Senior Member, IEEE*, Chung-You Lin, Jun-Jie Liaw, and Yung-Ruei Chang, *Member, IEEE*

Abstract—A newly designed zero-voltage-switching (ZVS) multi-input converter is proposed in this paper. The converter can boost the different voltages of two power sources to a stable output voltage. An auxiliary circuit is employed for achieving turn-on ZVS of all switches in the proposed converter. According to various situations, the operational states of the proposed converter can be divided into two states, including a single-power-supply and a dual-power-supply state. In the dual-power-supply state, the input circuits connected in series together with the designed pulsewidth modulation can greatly reduce the conduction loss of the switches. In addition, the effectiveness of the designed circuit topology and the ZVS properties are verified by experimental results, and the goal of high-efficiency conversion can be obtained.

Index Terms—High-efficiency conversion, multi-input converter, zero voltage switching (ZVS).

I. INTRODUCTION

IN ORDER to protect the natural environment of the Earth, the development of clean energy [1]–[3] without pollution has had a major representative role in the last decade. By accompanying the permission of the Kyoto Protocol, clean energies, such as fuel cell (FC), photovoltaic, and wind energies, etc., have been rapidly promoted. Due to the electric characteristics of clean energies, the generated power is critically affected by the climate or has slow transient responses, and the output voltage is easily influenced by load variations. Thus, a storage element is necessary to ensure proper operation of clean energies. Batteries or supercapacitors are usually taken as storage mechanisms for smoothing output power, startup transition, and various load conditions. The corresponding installed capacity of clean energies can be further reduced to save the cost of system purchasing and power supply. For these reasons, hybrid power-conversion systems have become interesting research topics for engineers and scientists at present.

Based on power electronics technique, the diversely developed power conditioners including dc–dc converters and dc–ac inverters are essential components for clean-energy applications. Generally, one power source needs a dc–dc converter either for raising the input voltage to a certain band [4], [5] or for regulating the input voltage to a constant dc-bus voltage. However, conventional converter structures have the

following disadvantages: 1) large size; 2) complex topology; and 3) expensive cost. In order to simplify circuit topology, improve system performance and reduce manufacturing cost, multi-input converters have received more attention in recent years [6]–[11].

Wai *et al.* [7], [8] presented multi-input converters with high step-up ratios, and the goal of high-efficiency conversion was obtained. However, these topologies are not economic for the nonisolated applications because of the complexity with numbers of electrical components. Tao *et al.* [9] and Matsuo *et al.* [10] utilized multiwinding-type transformers to accomplish the power-conversion target of multi-input sources. Although these topologies were designed based on the time-sharing concept, the complexity of driving circuits will be increased by the control techniques in [9] and [10]. Marchesoni and Vacca [11] investigated a newly designed converter with the series-connected input circuits to achieve the goal of multiple input power sources. The installation cost of the converter with few components was certainly reduced. The feature of [11] is that the conduction losses of switches can be greatly reduced, particularly in the dual-power-supply state. Unfortunately, the hard-switching problem and the huge reverse-recovery current within the output diode degrade the conversion efficiency as a traditional boost converter [4]. Giacomini *et al.* [12] proposed a dc–dc zero-voltage-switching (ZVS) pulsewidth-modulation (PWM) converter with active clamping. The soft commutation in all the switches was obtained by an additional active clamping circuit, and a small heat sink was used in this converter to reduce the weight, volume, and the final cost. However, the topology in [12] is only suitable for a single input power source.

In this paper, a high-efficiency ZVS multi-input converter is investigated, and this converter directly utilizes the current-source type applying to both input power sources. Based on the series-connected input circuits and the designed PWM driving signals, the conduction loss of the switches can be greatly reduced in the dual-power-supply state. An auxiliary circuit with a small inductor operated in the discontinuous conduction mode (DCM) is utilized for achieving turn-on ZVS of all the switches, and the huge reverse-recovery current of the output diode in the traditional boost converter [12] can be removed via the utilization of an auxiliary inductor series connected with a Schottky diode. In addition, an interleave method [13], [14] for two input inductor currents is used to alleviate the output voltage ripple. Consequently, the proposed converter can efficiently convert two power sources with different voltages to a stable dc-bus voltage. According to the power dispatch, this converter could be operated at two states, including a single-power-supply state and a dual-power-supply state. This paper is organized into four sections. Following the introduction in
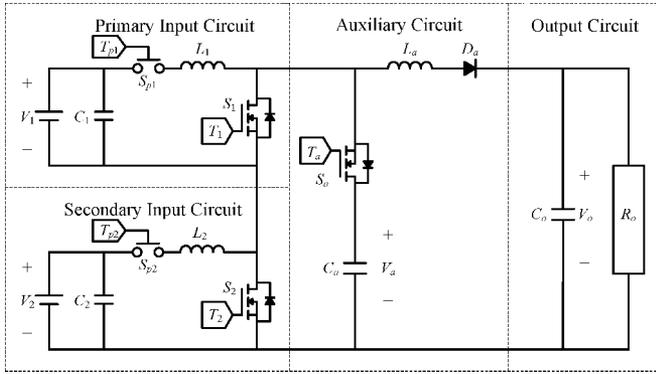
556

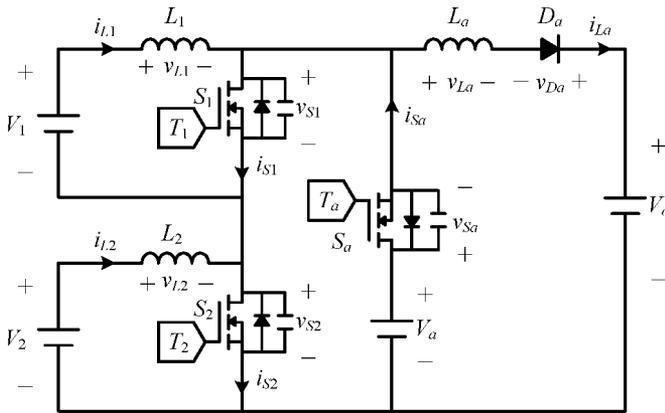Fig. 1. Circuit topology of high-efficiency multi-input converter.

Fig. 2. Equivalent circuit.

Section I, the topology and operation of the proposed high-efficiency multi-input converter are presented in Section II. In Section III, experimental results are provided to validate the effectiveness of the proposed converter. Conclusions are drawn in Section IV.

II. TOPOLOGY AND OPERATION OF MULTI-INPUT CONVERTER

Fig. 1 shows the circuit topology of the proposed ZVS multi-input converter. It contains four parts, including a primary input circuit, a secondary input circuit, an auxiliary circuit, and an output circuit. The major symbol representations are summarized as follows. V_1 denotes the primary input voltage. V_2 exhibits the secondary input voltage. S_{P1}, S_{P2}, T_{P1}, and T_{P2} express the power on/off switches and their driving signals produced by the power management. C_i, L_i, S_i, and T_i ($i = 1, 2$) represent individual capacitors, inductors, switches, and driving signals in the primary and secondary input circuits, respectively. C_a, L_a, and D_a are the auxiliary capacitor, inductor, and diode of the auxiliary circuit. S_a and T_a are the auxiliary switch and its driving signal, which is generated by the PWM. C_o, V_o, and R_o describe the output capacitor, voltage, and equivalent load.

For the convenience of analyses, the simplified equivalent circuit is shown in Fig. 2, and the directional definition of significant voltages and currents are labeled in this figure. The simplification in Fig. 2 is compliant with the following
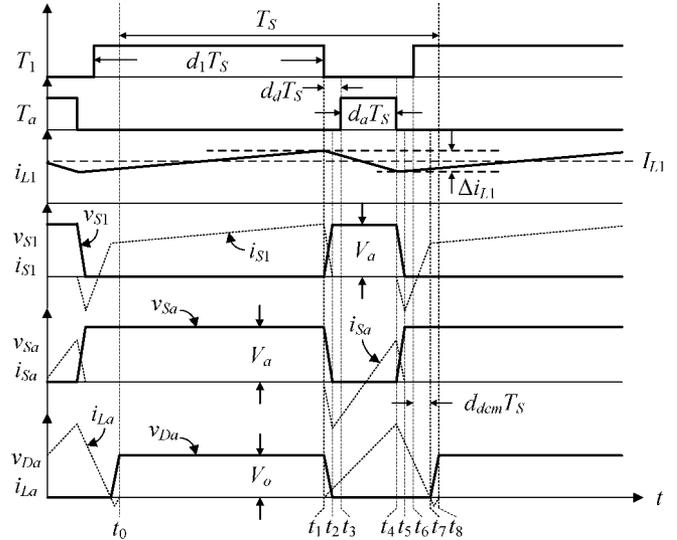

Fig. 3. Characteristic waveforms in single-power-supply state.

assumptions: 1) all power switches and diodes have ideal characteristics without considering voltage drops when these devices are conducted; 2) the capacitors C_a and C_o are large enough so that the voltage ripples due to switching are negligible and could be taken as constant voltage sources V_a and V_o; 3) the power on/off switches S_{P1} and S_{P2} are omitted. According to different power conditions, the operational states of the proposed converter can be divided into two states: a single-power-supply state with only one input power source and a dual-power-supply state with two input power sources. The detailed operational stages are described as follows.

A. Single-Power-Supply State

Depending on the power management for energy saving or failure protection, the proposed converter can be operated in the single-power-supply state. By turning off one power on/off switch S_{P1} or S_{P2} to cut off the connection between the power source and the converter, the other input power source V_2 or V_1 can supply alone to support the output demand. The primary input power supply is considered, for example, to explain how to operate in this state, i.e., switch S_{P2} is always turned off and switch S_2 is triggered all the while for minimizing the conduction loss. The switching period is defined as T_s. d_1 and d_a denote the duty cycles of switches S_1 and S_a, respectively. d_d and d_{dcm} present the duty cycles of the dead time and the freewheeling time of the auxiliary inductor. Note that the auxiliary inductor is designed to operate in the DCM. The characteristic waveforms and topological modes of the single-power-supply state are shown in Figs. 3 and 4, respectively. The complete operation modes in a switching period of the converter are discussed as follows.

Mode 1 [t_0-t_1]: At t_0, the auxiliary inductor current i_{La} returned to zero. Switch S_1 is continuously conducted, and the auxiliary switch S_a is still turned off. The primary inductor L_1 is linearly charged by the primary input voltage V_1. The auxiliary switch voltage v_{Sa} is equal to the auxiliary capacitor voltage V_a.
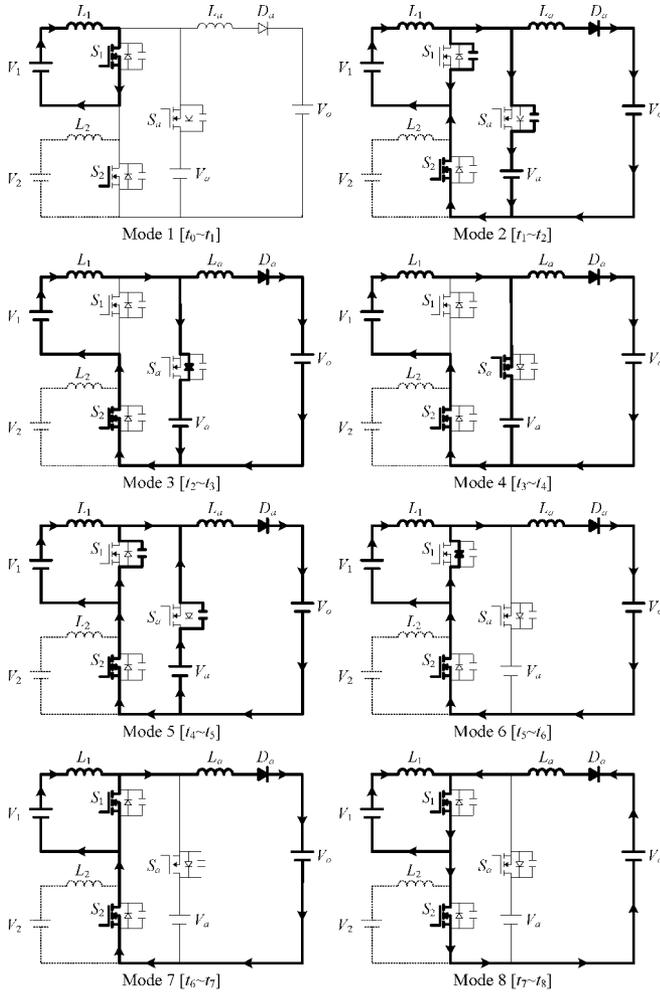
Fig. 4. Topological modes in single-power-supply state.

Mode 2 $[t_1-t_2]$: At t_1, switch S_1 is turned off and the parasitic capacitor of switch S_1 is charged by the primary inductor current i_{L1}. At the same time, the energy stored in the parasitic capacitor of the auxiliary switch S_a and the junction capacitance of the auxiliary diode D_a is also removed by the primary inductor current i_{L1}.

Mode 3 $[t_2-t_3]$: At t_2, the switch voltage v_{S1} is rising to the auxiliary capacitor voltage V_a, and the auxiliary switch voltage v_{Sa} is decreasing to zero. The body diode of the auxiliary switch S_a is conducted for receiving the primary inductor current i_{L1} to charge the auxiliary capacitor voltage V_a. Therefore, the switch current i_{Sa} is negative. Furthermore, the auxiliary inductor current i_{La} linearly increases, and the slope is dependent on the auxiliary inductor voltage v_{La}, which is equal to $V_a - V_o$. Continuously, the auxiliary diode D_a is conducted.

Mode 4 $[t_3-t_4]$: At t_3, the auxiliary switch S_a is turned on with ZVS because the body diode has been already conducted for carrying the primary inductor current i_{L1}. After the auxiliary inductor current i_{La} increases to be larger than the primary inductor current i_{L1}, the auxiliary switch current i_{Sa} becomes positive. The discharging current from the auxiliary capacitor, together with the primary inductor current i_{L1}, releases the stored energy to the output voltage V_o. During modes 2–4

$(t = t_1 - t_4)$, the time interval can be written as $(d_d + d_a)T_s$. The auxiliary inductor current i_{La}, the primary inductor current i_{L1}, and the auxiliary switch current i_{Sa} can be expressed as

$$i_{La}(t) = (V_a - V_o)(t - t_1)/L_a \tag{1}$$

$$i_{L1}(t) = (I_{L1} + 0.5\Delta i_{L1}) + (V_1 - V_a)(t - t_1)/L_1 \tag{2}$$

$$\begin{aligned}
i_{Sa}(t) &= i_{La}(t) - i_{L1}(t) \\
&= [(V_a - V_o)/L_a - (V_1 - V_a)/L_1] \\
&\quad \cdot (t - t_1) - (I_{L1} + 0.5\Delta i_{L1})
\end{aligned} \tag{3}$$

where I_{L1} is the average value of the primary inductor current i_{L1} and Δi_{L1} is the corresponding peak-to-peak current ripple. Note that the time interval $(t_1 - t_2)$ in mode 2 is extremely short so that it could be regarded as the same time in Fig. 4. At t_4, the maximum values of the auxiliary inductor current i_{La} and the auxiliary switch current i_{Sa} can be calculated as

$$i_{La}(t_4) = (V_a - V_o)(d_d + d_a)T_s/L_a \tag{4}$$

$$i_{Sa}(t_4) = (V_a - V_o)(d_d + d_a)T_s/L_a - (I_{L1} - 0.5\Delta i_{L1}). \tag{5}$$

According to the primary inductor voltage v_{L1}, the current ripple Δi_{L1} can be rewritten as

$$\Delta i_{L1} = (V_a - V_1)(d_d + d_a)T_s/L_1. \tag{6}$$

Mode 5 $[t_4-t_5]$: At t_4, the auxiliary switch S_a is turned off. Because the auxiliary inductor current i_{La} is greater than the primary inductor current i_{L1}, the parasitic capacitor of the auxiliary switch S_a is charged by the auxiliary inductor current i_{La} and the auxiliary switch voltage v_{Sa} rises. At the same time, the energy stored in the parasitic capacitor of switch S_1 will release to the output voltage V_o via the inductor current i_{La} and the switch voltage v_{S1} decreases.

Mode 6 $[t_5-t_6]$: At t_5, the switch current i_{Sa} falls down to zero and the switch voltage v_{Sa} rises to the auxiliary capacitor voltage V_a. In mode 6, the primary switch current i_{S1} can be represented as $i_{L1} - i_{La}$. Because the auxiliary inductor current i_{La} is still greater than the primary inductor current i_{L1}, the body diode of switch S_1 is conducted for carrying the differential current without strain. Furthermore, the auxiliary inductor voltage v_{La} is equal to $-V_o$, and the current i_{La} linearly decreases. The energy stored in the auxiliary inductor L_a starts to discharge into the output voltage V_o as freewheeling.

Mode 7 $[t_6-t_7]$: At t_6, switch S_1 is turned on with ZVS upon the condition that the auxiliary inductor current i_{La} is still larger than the primary inductor current i_{L1}. The auxiliary inductor current i_{La} continuously decreases with the slope $-V_o/L_a$. After the current i_{La} is smaller than the primary inductor current i_{L1}, the switch current i_{S1} is positive. During modes 5–7 $(t = t_4 - t_7)$, the time interval can be written as $(d_d + d_{dcm})T_s$. The auxiliary inductor current i_{La}, the primary

inductor current i_{L1}, and the first switch current i_{S1} can be expressed as

$$i_{La}(t) = [(V_a - V_o)(d_d + d_a)T_s - V_o(t - t_4)]/L_a \quad (7)$$

$$i_{L1}(t) = (I_{L1} - 0.5\Delta i_{L1}) + V_1(t - t_4)/L_1 \quad (8)$$

$$i_{S1}(t) = (I_{L1} - 0.5\Delta i_{L1}) + (V_1/L_1 + V_o/L_a)(t - t_4)$$
$$- (V_a - V_o)(d_d + d_a)T_s/L_a. \quad (9)$$

Note that the time interval $(t_4 - t_5)$ in mode 5 is extremely short so that it could be regarded as the same time.

Mode 8 $[t_7 - t_8]$: At t_7, the auxiliary inductor current i_{La} is equal to zero. Substituting $i_{La}(t_7) = 0$ into (7), the relation between the voltages V_a and V_o can be derived as

$$(V_a - V_o)(d_d + d_a) = V_o(d_d + d_{dcm}). \quad (10)$$

In this mode, the parasitic capacitor of the diode D_a is charged by the output voltage V_o with a small reverse-recovery current. As the diode voltage v_{Da} is rising to the output voltage V_o, the auxiliary inductor current i_{La} returns to zero. In the single-power-supply state with the primary input power, switch S_{P2} is always turned off and switch S_2 is triggered all the while. It means that switch S_2 works as a synchronous rectifier for avoiding the current to flow through its body diode and reducing the power losses in modes 2–8 of Fig. 4.

According to the volt-second balance theory [15], the voltage-second production of the primary inductor L_1 in a switching period should be equal to zero. Thus, one can obtain

$$V_1(d_1 + d_d)T_S + (V_1 - V_a)(d_a + d_d)T_S = 0 \quad (11a)$$

$$V_1 = V_a(d_a + d_d). \quad (11b)$$

Assume that the dead-time duty cycle d_d is much smaller than the duty cycle of switch d_1; the summation of the duty cycles d_1 and d_a approaches one. The relationships of the voltages in (10) and (11b) can be rewritten as

$$V_o = (1 - d_1)V_a/(1 + d_{dcm} - d_1) \quad (12a)$$

$$V_1 = (1 - d_1)V_a \quad (12b)$$

$$V_o/V_1 = 1/(1 + d_{dcm} - d_1). \quad (12c)$$

Because the average current of the output capacitor C_o should be zero over a switching period for a constant output voltage V_o, the equation of the balance can be expressed as

$$0.5(V_a - V_o)(1 - d_1)T_s(1 - d_1 + d_{dcm})/L_a = V_o/R_o. \quad (13)$$

From the algebraic operation via (12) and (13), the duty cycle and the voltage gain of the converter can be derived as

$$d_{dcm} = 0.5(1 - d_1)\left[\sqrt{1 + \frac{8L_a}{R_oT_s(1 - d_1)^2}} - 1\right] \quad (14a)$$

$$V_o = 2V_1/(1 - d_1)\left[1 + \sqrt{1 + \frac{8L_a}{R_oT_s(1 - d_1)^2}}\right]. \quad (14b)$$
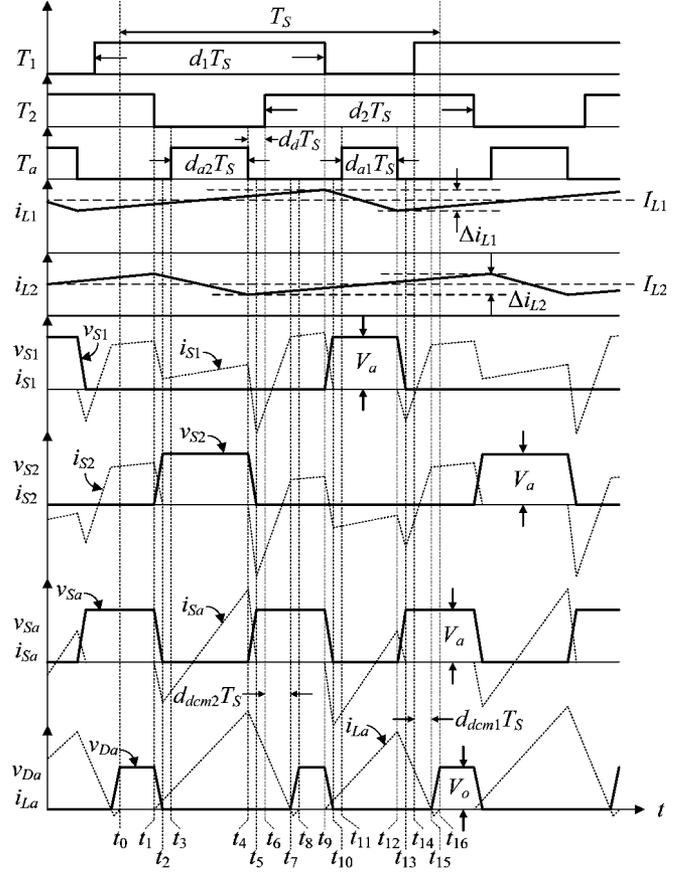

Fig. 5. Characteristic waveforms in dual-power-supply state.

By the similar derivation process, the voltage gain of the single-power-supply state with the secondary input power source also can be represented as

$$V_a = V_2/(1 - d_2) \quad (15a)$$

$$V_o = 2V_2/(1 - d_2)\left[1 + \sqrt{1 + \frac{8L_a}{R_oT_s(1 - d_2)^2}}\right] \quad (15b)$$

where d_2 denotes the duty cycle of switch S_2.

B. Dual-Power-Supply State

Depending on the power management for proper power output demand, the proposed converter can be operated in the dual-power-supply state with two input power sources. It can be taken as a superposition process of the primary and secondary input circuits. In this state, the summation of duty cycles d_1 and d_2 should be greater than one, i.e., each of duty cycles d_1 and d_2 is securely greater than 0.5. Moreover, the symbols d_{a1} and d_{a2} denote the first and the second duty cycles of switch S_a, respectively. d_{dcm1} and d_{dcm2} present the first and the second duty cycles of the freewheeling times of the auxiliary inductor. The auxiliary inductor is also designed to operate in the DCM. In order to explain the operational principle in the dual-power-supply state easily, the following theoretical analysis is based on the assumption of $i_{L1} > i_{L2} > |i_{L1} - i_{L2}|$, where $|\cdot|$ is the absolute operator. The characteristic waveforms and topological modes of the dual-power-supply state are shown in Figs. 5
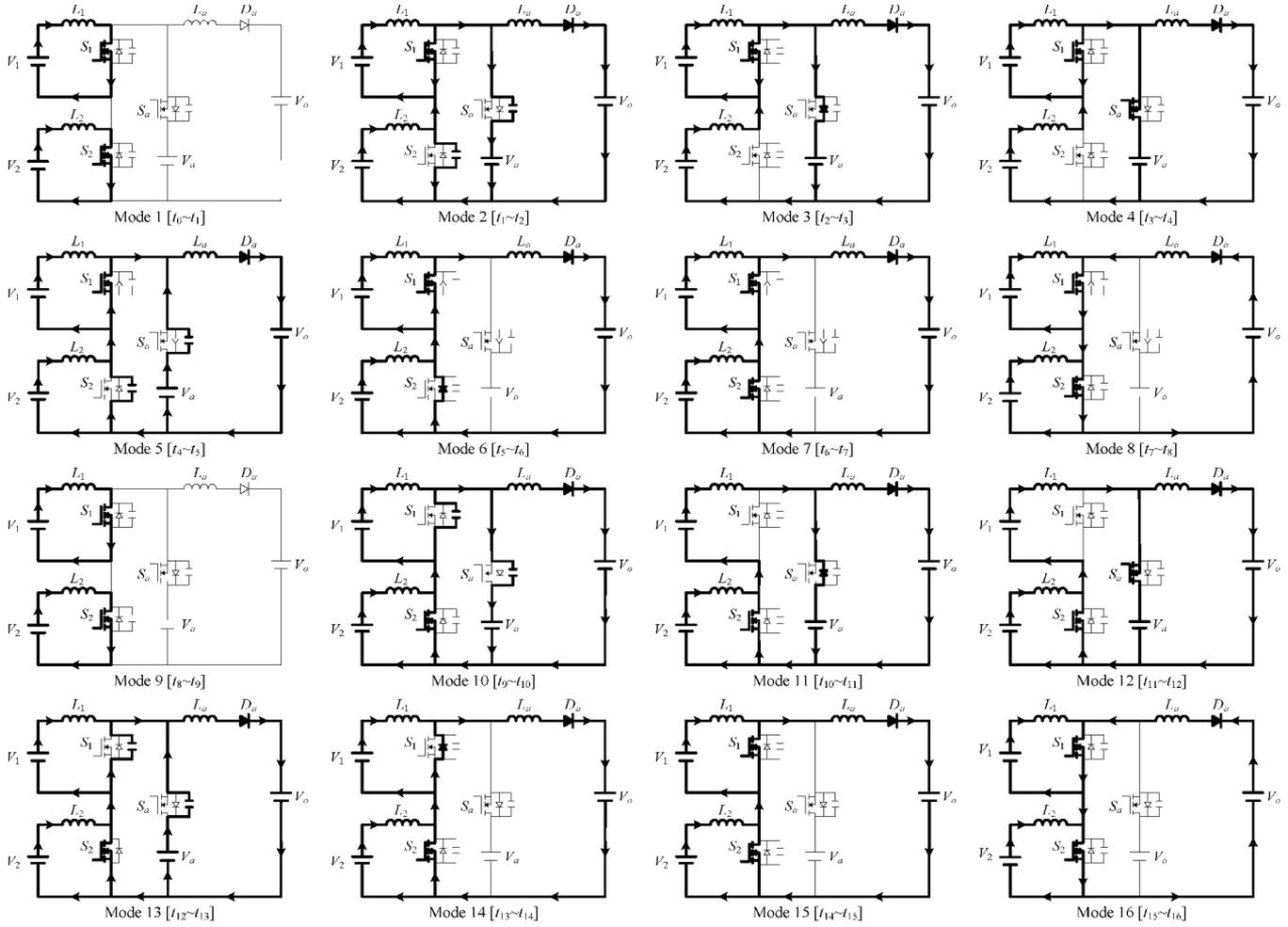
Fig. 6.   Topological modes in dual-power-supply state.

and 6, respectively. Note that, the time intervals in modes 2, 5, 10, and 13 are extremely short so that each interval could be regarded as the same time in Fig. 5. The operation modes in this state are discussed as follows.

Mode 1 [t_0-t_1]: At t_0, the auxiliary inductor current i_{La} returned to zero. Switches S_1 and S_2 are continuously conducted. The auxiliary switch S_a is still turned off. Inductors L_1 and L_2 are linearly charged by the input voltages V_1 and V_2, respectively.

Mode 2 [t_1-t_2]: At t_1, switch S_2 is turned off, and the parasitic capacitor of switch S_2 is charged by the secondary inductor current i_{L2}. At the same time, the energy stored in the parasitic capacitor of the auxiliary switch S_a and the junction capacitance of the auxiliary diode D_a is also removed by the secondary inductor current i_{L2}.

Mode 3 [t_2-t_3]: At t_2, the switch voltage v_{S2} is rising to the auxiliary capacitor voltage V_a and the auxiliary switch voltage v_{Sa} is decreasing to zero. The body diode of the auxiliary switch S_a is conducted for receiving the secondary inductor current i_{L2} to charge the auxiliary capacitor voltage V_a. Therefore, the switch current i_{Sa} is negative. Moreover, the auxiliary inductor current i_{La} linearly increases, and the slope is dependent on the auxiliary inductor voltage v_{La}, which is

equal to $V_a - V_o$. Continuously, the auxiliary diode D_a is conducted.

Mode 4 [t_3-t_4]: At t_3, the auxiliary switch S_a is turned on with ZVS. After the auxiliary inductor current i_{La} increases to be larger than the secondary inductor current i_{L2}, the auxiliary switch current i_{Sa} becomes positive. The discharging current from the auxiliary capacitor together with the secondary inductor current i_{L2} releases the stored energy to the output voltage V_o. During modes 2–4 ($t = t_1-t_4$), the time interval can be written as $(d_d + d_{a2})T_s$. The auxiliary inductor current i_{La}, the secondary inductor current i_{L2}, and the auxiliary switch current i_{Sa} can be expressed as

$$i_{La}(t) = (V_a - V_o)(t - t_1)/L_a \tag{16}$$

$$i_{L2}(t) = (I_{L2} + 0.5\Delta i_{L2}) + (V_2 - V_a)(t - t_1)/L_2 \tag{17}$$

$$i_{Sa}(t) = i_{La}(t) - i_{L2}(t)$$
$$= [(V_a - V_o)/L_a - (V_2 - V_a)/L_2]$$
$$\cdot (t - t_1) - (I_{L2} + 0.5\Delta i_{L2}) \tag{18}$$

where I_{L2} is the average value of the secondary inductor current i_{L2} and Δi_{L2} is the corresponding peak-to-peak current ripple. At t_4, the local maximum values of the auxiliary inductor current i_{La} and the auxiliary switch current i_{Sa} can be calculated as

$$i_{La}(t_4) = (V_a - V_o)(d_d + d_{a2})T_s/L_a \tag{19}$$

$$i_{Sa}(t_4) = (V_a - V_o)(d_d + d_{a2})T_s/L_a - (I_{L2} - 0.5\Delta i_{L2}). \tag{20}$$

According to the secondary inductor voltage v_{L2}, the current ripple Δi_{L2} can be rewritten as

$$\Delta i_{L2} = (V_a - V_2)(d_d + d_{a2})T_s/L_2. \tag{21}$$

In addition, by applying Kirchhoff's current law, the current loop equation is given by $i_{L1} = i_{S1} + i_{L2}$. The switch current i_{S1} can be expressed as $i_{L1} - i_{L2}$, and it is positive so far due to the current relationship $i_{L1} > i_{L2}$. By the topological design and switching mechanism, the conduction loss of switch S_1 sustaining all the primary inductor current i_{L1} can be effectively reduced, particularly in the low-voltage high-current clean-energy applications.

Mode 5 [t_4-t_5]: At t_4, the auxiliary switch S_a is turned off. Because the auxiliary inductor current i_{La} is greater than the secondary inductor current i_{L2}, the parasitic capacitor of the auxiliary switch S_a is charged by the auxiliary inductor current i_{La} and the auxiliary switch voltage v_{Sa} rises. At the same time, the energy stored in the parasitic capacitor of switch S_2 will be released to the output voltage V_o via the inductor current i_{La} and the switch voltage v_{S2} decreases.

Mode 6 [t_5-t_6]: At t_5, the switch current i_{Sa} falls down to zero and the switch voltage v_{Sa} rises to the auxiliary capacitor voltage V_a. In mode 6, the primary switch current i_{S1} can be represented as $i_{L1} - i_{La}$ and the secondary switch current i_{S2} can be represented as $i_{L2} - i_{La}$. Because the auxiliary inductor current i_{La} is greater than the inductor current i_{L2}, the body diode of switch S_2 is conducted for carrying the differential current without strain. The auxiliary inductor current i_{La} is also greater than the inductor current i_{L1}, such that both the switches' currents i_{S1} and i_{S2} are negative. Furthermore, the auxiliary inductor voltage v_{La} is equal to $-V_o$, and the current i_{La} linearly decreases. The energy stored in the auxiliary inductor L_a starts to discharge into the output voltage V_o as freewheeling.

Mode 7 [t_6-t_7]: At t_6, switch S_2 is turned on with ZVS upon the condition that the auxiliary inductor current i_{La} is still larger than the secondary inductor current i_{L2}. The auxiliary inductor current i_{La} continuously decreases with the slope $-V_o/L_a$. After the current i_{La} is smaller than the secondary inductor current i_{L2}, the switch current i_{S2} is positive. In the same way, the switch current i_{S1} becomes positive as well as i_{S2}. During modes 5–7 ($t = t_4-t_7$), the time interval can be written as $(d_d + d_{dcm2})T_s$. The auxiliary inductor current i_{La},

the secondary inductor current i_{L2}, and the secondary switch current i_{S2} can be expressed as

$$i_{La}(t) = [(V_a - V_o)(d_d + d_{a2})T_s - V_o(t - t_4)]/L_a \tag{22}$$

$$i_{L2}(t) = (I_{L2} - 0.5\Delta i_{L2}) + V_2(t - t_4)/L_2 \tag{23}$$

$$i_{S2}(t) = (I_{L2} - 0.5\Delta i_{L2}) + (V_2/L_2 + V_o/L_a)(t - t_4) \\ - (V_a - V_o)(d_d + d_{a2})T_s/L_a. \tag{24}$$

Mode 8 [t_7-t_8]: At t_7, the auxiliary inductor current i_{La} is equal to zero. By substituting $i_{La}(t_7) = 0$ into (22), the relation between the voltages V_a and V_o can be derived as

$$(V_a - V_o)(d_d + d_{a2}) = V_o(d_d + d_{dcm2}). \tag{25}$$

In this mode, the parasitic capacitor of the diode D_a is charged by the output voltage V_o with a small reverse-recovery current.

Mode 9 [t_8-t_9]: At t_8, the auxiliary inductor current i_{La} returns to zero. Switches S_1 and S_2 are continuously conducted. Mode 9 is similar to mode 1.

Mode 10 [t_9-t_{10}]: At t_9, switch S_1 is turned off and the parasitic capacitor of switch S_1 is charged by the primary inductor current i_{L1}. The procedures of the auxiliary switch S_a and diode D_a are similar to the ones in mode 2.

Mode 11 [$t_{10}-t_{11}$]: The body diode of the auxiliary switch S_a is conducted for carrying the primary inductor current i_{L1} to charge the auxiliary capacitor. The auxiliary inductor current i_{La} linearly increases with the slope $(V_a - V_o)/L_a$. Continuously, the auxiliary diode D_a is conducted.

Mode 12 [$t_{11}-t_{12}$]: At t_{11}, the auxiliary switch S_a is turned on with ZVS. After the auxiliary inductor current i_{La} increases to be larger than the primary inductor current i_{L1}, the auxiliary switch current i_{Sa} becomes positive. The discharging current from the auxiliary capacitor together with the primary inductor current i_{L1} releases the stored energy to the output voltage V_o. During modes 10–12 ($t = t_9-t_{12}$), the time interval can be written as $(d_d + d_{a1})T_s$. The auxiliary inductor current i_{La}, the primary inductor current i_{L1}, and the auxiliary switch current i_{Sa} can be expressed as

$$i_{La}(t) = (V_a - V_o)(t - t_9)/L_a \tag{26}$$

$$i_{L1}(t) = (I_{L1} + 0.5\Delta i_{L1}) + (V_1 - V_a)(t - t_9)/L_1 \tag{27}$$

$$i_{Sa}(t) = i_{La}(t) - i_{L1}(t) \\ = [(V_a - V_o)/L_a - (V_1 - V_a)/L_1] \\ \cdot (t - t_9) - (I_{L1} + 0.5\Delta i_{L1}). \tag{28}$$

At t_{12}, the local maximum values of the auxiliary inductor current i_{La} and the auxiliary switch current i_{Sa} can be calculated as

$$i_{La}(t_{12}) = (V_a - V_o)(d_d + d_{a1})T_s/L_a \tag{29}$$

$$i_{Sa}(t_{12}) = (V_a - V_o)(d_d + d_{a1})T_s/L_a - (I_{L1} - 0.5\Delta i_{L1}). \tag{30}$$

The current ripple Δi_{L1} can be rewritten as

$$\Delta i_{L1} = (V_a - V_1)(d_d + d_{a1})T_s/L_2. \tag{31}$$

In addition, the switch current i_{S2} can be expressed as $i_{L2} - i_{L1}$, and it is negative. The conduction loss of switch S_2 can be effectively reduced.

Mode 13 $[\boldsymbol{t_{12}-t_{13}}]$: At t_{12}, the auxiliary switch S_a is turned off. Because the auxiliary inductor current i_{La} is greater than the primary inductor current i_{L1}, the parasitic capacitor of the auxiliary switch S_a is charged by the auxiliary inductor current i_{La}. At the same time, the energy stored in the parasitic capacitor of switch S_1 will be released to the output voltage V_o via the inductor current i_{La}.

Mode 14 $[\boldsymbol{t_{13}-t_{14}}]$: At t_{13}, the switch current i_{Sa} falls down to zero and the switch voltage v_{Sa} rises to the auxiliary capacitor voltage V_a. Similar to mode 6, both the switches' currents i_{S1} and i_{S2} are negative. The energy stored in auxiliary inductor L_a starts to discharge into the output voltage V_o as freewheeling.

Mode 15 $[\boldsymbol{t_{14}-t_{15}}]$: At t_{14}, switch S_1 is turned on with ZVS. The auxiliary inductor current i_{La} continuously decreases with the slope $-V_o/L_a$. After the current i_{La} is smaller than the primary inductor current i_{L1}, the switch current i_{S1} is positive. By the same way, the switch current i_{S2} becomes positive as well as i_{S1}. During modes 13–15 ($t = t_{12}-t_{15}$), the time interval can be written as $(d_d + d_{\text{dcm1}})T_s$. The auxiliary inductor current i_{La}, the primary inductor current i_{L1}, and the primary switch current i_{S1} can be expressed as

$$i_{La}(t) = [(V_a - V_o)(d_d + d_{a1})T_s - V_o(t - t_{12})]/L_a \quad (32)$$

$$i_{L1}(t) = (I_{L1} - 0.5\Delta i_{L1}) + V_1(t - t_{12})/L_1 \quad (33)$$

$$i_{S1}(t) = (I_{L1} - 0.5\Delta i_{L1}) + (V_1/L_1 + V_o/L_a)(t - t_{12})$$
$$- (V_a - V_o)(d_d + d_{a1})T_s/L_a. \quad (34)$$

Mode 16 $[\boldsymbol{t_{15}-t_{16}}]$: At t_{15}, the auxiliary inductor current i_{La} is equal to zero. By substituting $i_{La}(t_{15}) = 0$ into (32), the relation between the voltages V_a and V_o can be derived as

$$(V_a - V_o)(d_d + d_{a1}) = V_o(d_d + d_{\text{dcm1}}). \quad (35)$$

Mode 16 is similar to mode 8 as well as the reverse-recovery time of the auxiliary diode D_a.

According to the volt-second balance theory [15], the voltage-second productions of the inductors L_1 and L_2 in a switching period should be equal to zero. Thus, one can obtain

$$V_1(d_1 + d_d)T_S + (V_1 - V_a)(d_{a1} + d_d)T_S = 0 \quad (36a)$$

$$V_2(d_2 + d_d)T_S + (V_2 - V_a)(d_{a2} + d_d)T_S = 0 \quad (36b)$$

$$V_1 = (d_{a1} + d_d)V_a \quad (36c)$$

$$V_2 = (d_{a2} + d_d)V_a. \quad (36d)$$

Assuming that the dead-time duty cycle d_d is much smaller than the duty cycles of switches d_1 and d_2, the relationships of the voltages in (25), (35), (36b), and (36d) can be rewritten as

$$V_o = (1 - d_1)V_a/(1 + d_{\text{dcm1}} - d_1)$$
$$= (1 - d_2)V_a/(1 + d_{\text{dcm2}} - d_2) \quad (37a)$$

$$V_a = V_1/(1 - d_1) = V_2/(1 - d_2) \quad (37b)$$

$$V_o/V_1 = 1/(1 + d_{\text{dcm1}} - d_1) \quad (37c)$$

$$V_o/V_2 = 1/(1 + d_{\text{dcm2}} - d_2). \quad (37d)$$

Because the average current of the output capacitor C_o should be zero over a switching period for a constant output voltage V_o, the equation of the balance can be expressed as shown at the bottom of the page. From the algebraic operation via (37) and (38), the duty cycles and the voltage gain of the converter can be derived as

$$d_{\text{dcm1}} = 0.5(1 - d_1)\left[\sqrt{1 + \frac{8L_a}{R_o T_s d_x}} - 1\right] \quad (39a)$$

$$d_{\text{dcm2}} = 0.5(1 - d_2)\left[\sqrt{1 + \frac{8L_a}{R_o T_s d_x}} - 1\right] \quad (39b)$$

$$V_o = 2V_1 \left/ \left[(1 - d_1)\left(1 + \sqrt{1 + \frac{8L_a}{R_o T_s d_x}}\right)\right]\right.$$
$$= 2V_2 \left/ \left[(1 - d_2)\left(1 + \sqrt{1 + \frac{8L_a}{R_o T_s d_x}}\right)\right]\right. \quad (39c)$$

where the duty cycle d_x is defined as $[(1 - d_1)^2 + (1 - d_2)^2]$. From (39c), the following can be obtained:

$$V_1/(1 - d_1) = V_2/(1 - d_2). \quad (40)$$

Equations (39c) and (40) state that the proposed converter can simultaneously boost both input power sources with different voltage levels to a stable output voltage via controlling the driving signals of switches T_1, T_2, and T_a. Moreover, there exists only one pair of the duty cycles d_1 and d_2 according to the input voltages.

Fig. 7 shows a circuit variation of the proposed converter with the same electrical components as Fig. 1. In the single-power-supply state, the driving signals of switches T_1 and T_a are shown in Fig. 3. By the same analysis, the voltage gain of this converter can be derived as (14b) or (15b). In the dual-power state, the driving signals T_1, T_2, and T_a are given shown

$$\frac{[(1 - d_1)(1 - d_1 + d_{\text{dcm1}}) + (1 - d_2)(1 - d_2 + d_{\text{dcm2}})](V_a - V_o)T_s}{2L_a} = V_o/R_o \quad (38)$$
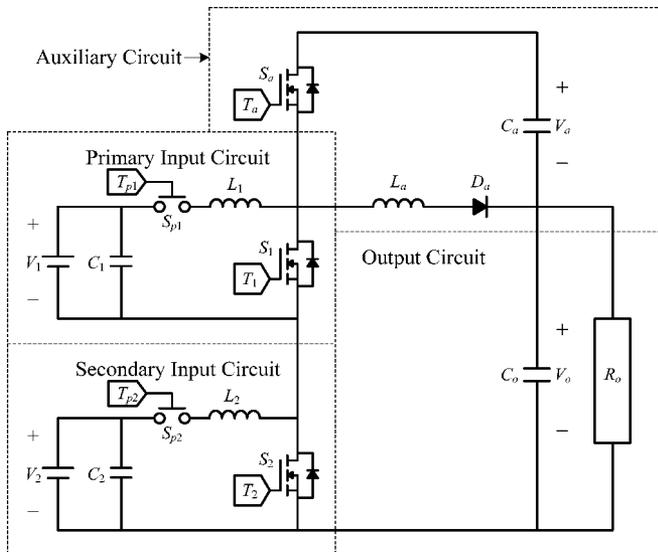
Fig. 7.   Circuit variation of high-efficiency multi-input converter.

in Fig. 5, and the voltage gain can be derived as (39c). The major difference between these two circuit topologies in Figs. 1 and 7 is the auxiliary capacitor voltage V_a, which, in the single- and dual-power states, are respectively given as

$$V_a = V_1 \frac{\sqrt{1 + \frac{8L_a}{R_o T_s (1-d_1)^2}} - 1}{(1 - d_1)\left[1 + \sqrt{1 + \frac{8L_a}{R_o T_s (1-d_1)^2}}\right]} \quad (41)$$

$$V_a = \frac{V_1 \left[\sqrt{1 + \frac{8L_a}{R_o T_s d_x}} - 1\right]}{\left[(1 - d_1)\left(1 + \sqrt{1 + \frac{8L_a}{R_o T_s d_x}}\right)\right]}$$

$$= \frac{V_2 \left[\sqrt{1 + \frac{8L_a}{R_o T_s d_x}} - 1\right]}{\left[(1 - d_2)\left(1 + \sqrt{1 + \frac{8L_a}{R_o T_s d_x}}\right)\right]}. \quad (42)$$

By comparing (41) and (42) to (12b) and (37b), the auxiliary capacitor voltage V_a is obviously reduced in the topology shown in Fig. 7. Nevertheless, this circuit variation also can efficiently convert two different input voltages to a stable output voltage.

In Figs. 1 and 7, the circuit framework can efficiently convert two different input voltages to a stable output voltage, but it has not a regenerative option. This drawback limits the possibility to use it in electric vehicles (EVs). Considering an application in EVs, a regenerative option is usually required while the EV brakes to recycle the regenerative braking energy without thermodissipation. The proposed multi-input topologies shown in Figs. 1 and 7 could permit bidirectional power by replacing the auxiliary diode (D_a) with an active switch. In this way, the energy utility and efficiency can be further raised. It is worthy to continuously investigate in the future research.

III. EXPERIMENTAL RESULTS

In order to verify the effectiveness of the proposed ZVS multi-input converter, the corresponding experimental results

are provided in this section. A power supply is used to emulate an FC taken as the primary power source with the properties of low voltage and high current, and the input voltage range is 10–14 V. Note that, the summation of duty cycles d_1 and d_2 should be greater than one for regular operation in the dual-power-supply state. Thus, each of duty cycles d_1 and d_2 should be bounded from a minimum value $d_{\min}$ to a maximum value $d_{\max}$. The minimum duty cycle $d_{\min}$ is designed to 0.55 slightly higher than a half of one, and the maximum duty cycle $d_{\max}$ is designed to 0.8 to avoid the lack of freewheeling time of the auxiliary inductor operating in DCM. According to the relation between input voltages and duty cycles in (40), the two input voltages should be in the same level. Therefore, the voltage of a battery module is chosen as 10 V for the secondary power source. EVs [16]–[18] have become reality nowadays due to the technical improvements of power electronics and energy storage devices. Comparing with the traditional vehicle with only an internal combustion engine, the EVs have a better efficiency and more economic fuel utilization. For this reason, this prototype is designed to deliver a constant dc output for a motor driver of a lightweight EV (LEV), such as an electric scooter or an electric bicycle. According to this LEV application, the desired output voltage is set at 30 V in this study.

The volumes and weights of the inductors usually take the most of those in the converter, and the overall cost is also based on the prices of these passive components. Thus, the design of the inductor value becomes a key factor of the proposed converter, particularly the auxiliary inductor L_a in the auxiliary circuit for proper operation. The design procedure of the inductors (L_1 and L_2) in the primary and secondary input circuits follows the conventional design method of a boost converter via considering an acceptable ripple current drawn by the input power source [15]. In this study, the values of $L_1 = 36$ μH and $L_2 = 52$ μH are selected. The auxiliary capacitor voltage V_a shown in (12b) and (37b) has a maximum value of 70 V in the theoretical analysis because of the maximum duty cycle $d_{\max} = 0.8$ and the maximum input voltage $V_{1,\max} = 14$ V. Therefore, the auxiliary switch S_a is chosen as a MOSFET IRFP2907 with a breakdown voltage of 75 V. According to mode 7 in the single-power-supply state, the discontinuous conduction period $(d_{\mathrm{dcm}} T_s)$ should be less than the turned-on period of switch $(d_1 T_s)$ in Fig. 3. By considering a maximum output power $P_o = 500$ W ($R_o = 1.8$ Ω) with the minimum input voltage $V_{1,\min} = 10$ V and the switching period $T_s = 25$ μs in the single-power-supply state, the auxiliary inductor L_a should be smaller than 28.8 μH according to (14a) and $d_{\max} = 0.8$. Moreover, the discontinuous conduction periods $d_{\mathrm{dcm}1} T_s$ and $d_{\mathrm{dcm}2} T_s$ shown in Fig. 5 should be both smaller than the overlap period $0.5(d_1 + d_2 - 1)$ while switches S_1 and S_2 are turned on in the dual-power-supply state. For the worst case, to ensure the DCM property of the auxiliary inductor current (i.e., the lowest input voltage of 10 V and the highest output power of 1000 W with the maximum duty cycle $d_{\max} = 0.8$), (39a) and (39b) limit the value of the auxiliary inductor to $L_a < 6.75$ μH. In addition, the converter should have the ability to provide an output voltage of 30 V for satisfying the experimental prototype. According to the maximum duty cycle

Components	Symbols	Parameters
Primary inductor	L_1	36 μH
Secondary inductor	L_2	52 μH
Auxiliary inductor	L_a	1.5 μH
Primary capacitor	C_1	2200 μF×4
Secondary capacitor	C_2	2200 μF×4
Auxiliary capacitor	C_a	1000 μF×2
Output capacitor	C_o	2200 μF×2
Switching frequency	f_s	40kHz
Switches	S_1, S_2, and S_a	IRFP2907
Diode	D_a	SB20100

$d_{\max} = 0.8$, the nominal primary input voltage $V_1 = 12$ V, and (14b), the condition for the auxiliary inductor $L_a < 1.8$ μH should hold to cope with the variation of the input voltage. Based on the aforementioned constraint, the value of the auxiliary inductor is chosen as $L_a = 1.5$ μH to compensate the nonideal electric characteristic and guarantee the voltage gain of the proposed multi-input converter.

For solving the problem of the output voltage variance with different loads, a proportional–integral (PI) feedback controller is utilized to ensure the system stability of the proposed converter and a digital signal processor (DSP) TMS320F2812 manufactured by Texas Instruments, Inc. is adopted to achieve this goal of feedback control. The driving signals are generated by the DSP and peripheral logic circuits. The prototype with the specifications given in Table I is designed to illustrate the effectiveness of the proposed converter. In addition, considering the dual-power-supply state, the converter has the theoretical maximum efficiency while the two input power sources have the same voltages and input powers because the conducting losses of switches S_1 and S_2 can be greatly reduced. Consequently, the proposed converter can also be applied for a single power source to obtain high-efficiency conversion by splitting the input power.

A. Single-Power-Supply State

For examining the performance of the single-power-supply state with the primary input power source, the experimental results with an emulated FC stack of 12 V and an output power of 320 W are shown in Fig. 8. The proposed converter under voltage control indeed produces a constant output voltage of 30 V via the DSP module written within a PI feedback control law.

Fig. 8(a) shows the driving signal T_1, the auxiliary capacitor voltage V_a, the output voltage V_o, and the primary inductor current i_{L1}. The auxiliary capacitor voltage V_a is nearly a constant voltage of 45 V, and the output voltage V_o is kept at 30 V as a stable dc output under the PI feedback control. The primary inductor current i_{L1} with an average value of 29.2 A is continuously charged and discharged in the continuous conduction mode (CCM), so that the current draw from the FC is always positive with a small current ripple for avoiding the life-cycle degradation. The driving signals T_1 and T_a and the switch voltage v_{S1} and current i_{S1} are shown in Fig. 8(b). The driving signals (T_1 and T_a) appear complemen-
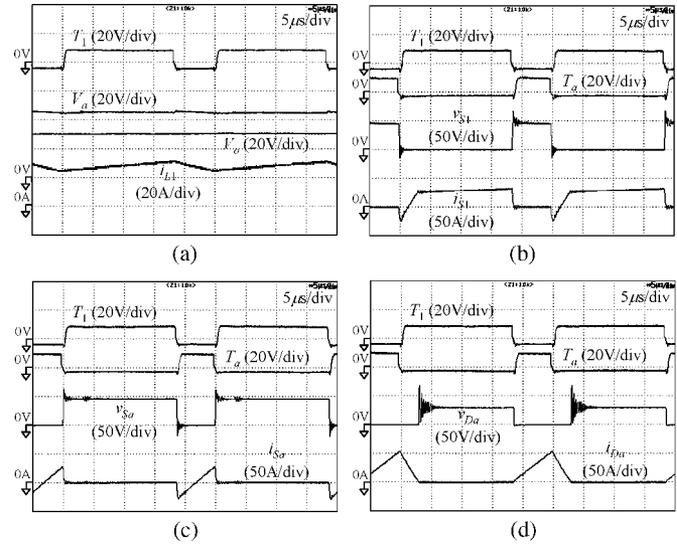

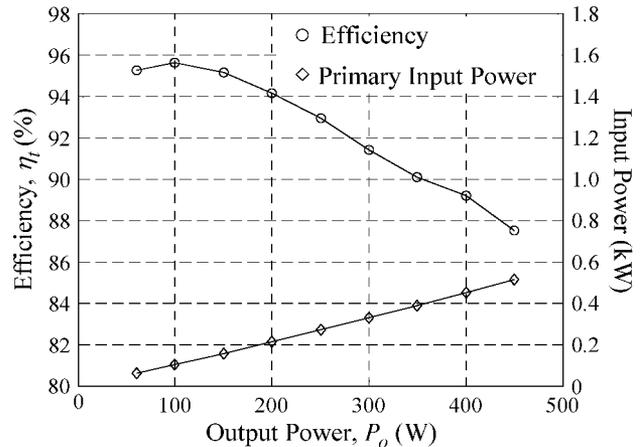Fig. 8. Experimental results at signal power supply state with 320-W output power.

Fig. 9. Conversion efficiency at signal power supply state.

tarily. By observing the switch voltage v_{S1} and current i_{S1}, the characteristic of turning on with ZVS is obvious due to the fact that the current is negative before the switch is turned on. Fig. 8(c) shows the driving signals (T_1 and T_a) and the switch voltage v_{Sa} and current i_{Sa}. The ZVS turn-on of switch S_a can also be achieved. The auxiliary capacitor C_a receives the primary inductor current i_{L1} at first, and then, the energy is released to the output terminal by the positive current i_{Sa}. Fig. 8(d) shows the driving signals (T_1 and T_a) and the diode voltage v_{Da} and current i_{Da}. It states that the diode current i_{Da} climbs with the slope $(V_a - V_o)/L_a$ and falls with the slope V_o/L_a. Moreover, the phenomenon of a huge reverse-recovery current disappears via the utilization of an auxiliary inductor series connected with a Schottky diode when the diode current falls to zero in comparison with the traditional step-up converters.

Fig. 9 shows the conversion efficiency η_t of the proposed converter operated at the single-power-supply state. The measured conditions are set with a primary input power source of 12 V and a constant output voltage of $V_o = 30$ V. From the experimental results, the maximum efficiency is
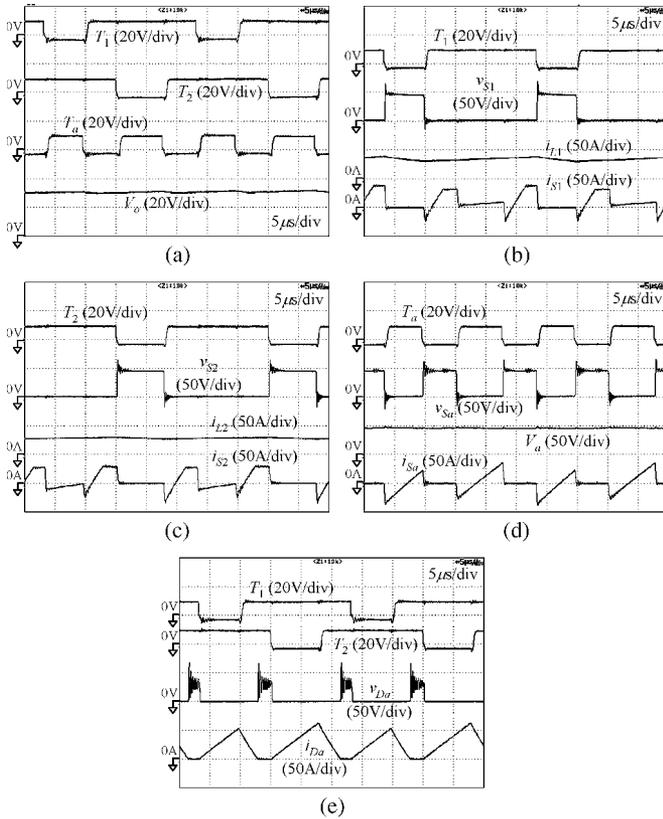
Fig. 10. Experimental results at dual-power-supply state with 720-W output power.

Fig. 11. Conversion efficiency at dual-power-supply state.

measured to be about 95.6% due to the ZVS property of all switches. The aforementioned experimental results agree well with those obtained from theoretical analyses given in Section II-A.

B. Dual-Power-Supply State

The experimental results of the dual-power-supply state with an emulated FC stack of 12 V, a battery module of 10 V, and an output voltage of 30 V are shown in Fig. 10. For the experimental condition, the FC stack is set to supply 400 W and the overall output power is preset as 720 W. It means that the power of the battery module of 376 W is expected possibly by measuring a conversion efficiency of 92.8%. The output voltage is maintained at the desired voltage of 30 V by a PI voltage controller via controlling switch S_2, and the FC continuously delivers 400 W by a PI current controller for the primary inductor current i_{L1} via controlling switch S_1. By implementing the PI feedback control laws in the DSP module, the goals of constant output voltage and specific primary input power can be concurrently achieved and verified by the following experimental results.

Fig. 10(a) shows the driving signals (T_1, T_2, and T_a) and the output voltage V_o. The driving signals satisfy the theoretical ones as shown in Fig. 6, and the output voltage V_o can be regulated at 30 V in the dual-power-supply state. The driving signal T_1, the primary inductor current i_{L1} with an average value of 33.3 A, and the switch voltage v_{S1} and current i_{S1} are shown in Fig. 10(b). Moreover, the driving signal T_2,
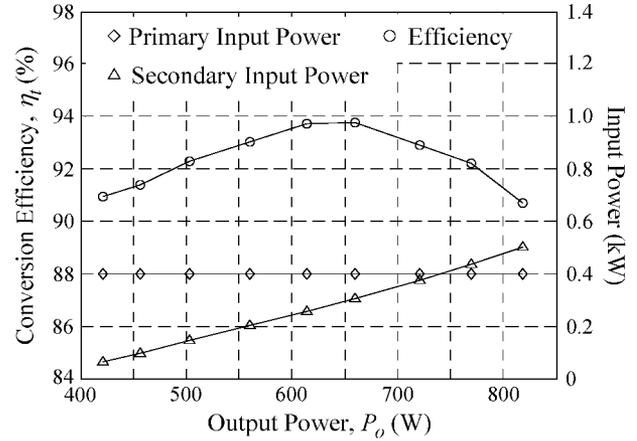
the secondary inductor current i_{L2} with an average value of 37.6 A, and the switch voltage v_{S2} and current i_{S2} are shown in Fig. 10(c). Both the inductors L_1 and L_2 are charged and discharged by turns in the CCM so that the currents i_{L1} and i_{L2} rise and fall behind the horizontal. By observing the switch voltages and currents in Fig. 10(b) and (c), the characteristics of turning on with ZVS of switches S_1 and S_2 are obvious. In addition, the switch current i_{S1} is equal to the primary inductor current i_{L1} when switch S_1 is turned on. After switch S_2 is turned on, the present switch current i_{S1} falls to $i_{L1} - i_{L2}$. On the other hand, the switch current i_{S2} appears negative and equal to $i_{L2} - i_{L1}$ after switch S_1 is turned on, and it reveals that the conduction losses of the switches are indeed reduced. Fig. 10(d) shows the driving signal T_a, the auxiliary capacitor voltage V_a, and the switch voltage v_{Sa} and current i_{Sa}. The fact that the auxiliary capacitor voltage is nearly constant agrees with the assumption in Section II. The ZVS turn-on of switch S_a with a negative starting current provides a path for the inductor current i_{L1} or i_{L2}. The different initial negative values of the current i_{Sa} indicate the peak values of the inductor currents i_{L1} and i_{L2}. Fig. 10(e) shows the driving signals (T_1 and T_2) and the diode voltage v_{Da} and current i_{Da}. The diode current i_{Da} appears linearly rising and falling in the DCM for charging the output capacitor.

Fig. 11 shows the conversion efficiency η_t of the proposed multi-input converter operated at the dual-power-supply state. The efficiency of the proposed converter is defined as the output power divided by the summation of the input powers. The operation conditions are set with a constant 400-W power produced by a primary input power source of 12 V and a secondary input power source of 10 V. From the experimental results, the maximum efficiency is measured to be about 93.8% because the conduction loss can be effectively reduced by the proposed topology and switching mechanism. The aforementioned experimental results agree well with those obtained from theoretical analyses given in Section II-B.

IV. CONCLUSION

This study has successfully developed a ZVS multi-input converter with hybrid power sources including an FC stack and

a battery module. The effectiveness of this converter is also verified by the experimental results. In the single-power-supply state, the property of ZVS turn-on of all switches guarantees that switching losses can be reduced. In the dual-power-supply state, the conduction loss can be effectively reduced by the topological design of series connection of two input circuits. Furthermore, the reverse-recovery current of the output diode is slight via a Schottky diode and the switching losses of the switches are effectively reduced. The maximum efficiency of the proposed converter operated in both operational states is higher than 93.8%. This new converter topology provides designers with an alternative choice to simultaneously convert hybrid power sources, particularly in the clean-energy applications with low-voltage and high-current inputs. In addition, the proposed high-efficiency multi-input converter also can work well in high-voltage-level applications because the switching loss, which is proportional to the square of the switch voltage, can be greatly reduced due to the ZVS property.

REFERENCES

[1] S. Al-Hallaj, "More than enviro-friendly: Renewable energy is also good for the bottom line," *IEEE Power Energy Mag.*, vol. 2, no. 3, pp. 16–22, May/Jun. 2004.

[2] P. Fairley, "The greening of GE," *IEEE Spectrum*, vol. 42, no. 7, pp. 28–33, Jul. 2005.

[3] R. C. Dugan, T. S. Key, and G. J. Ball, "Distributed resources standards," *IEEE Ind. Appl. Mag.*, vol. 12, no. 1, pp. 27–34, Jan./Feb. 2006.

[4] M. B. Camara, H. Gualous, F. Gustin, and A. Berthon, "Design and new control of DC/DC converter to share energy between supercapacitors and batteries in hybrid vehicles," *IEEE Trans. Veh. Technol.*, vol. 57, no. 5, pp. 2721–2735, Sep. 2008.

[5] T. Bhattacharya, "Multiphase bidirectional flyback converter topology for hybrid electric vehicles," *IEEE Trans. Ind. Electron.*, vol. 56, no. 1, pp. 78–83, Jan. 2009.

[6] Y. M. Chen, Y. C. Liu, S. C. Hung, and C. S. Cheng, "Multi-input inverter for grid-connected hybrid PV/wind power system," *IEEE Trans. Power Electron.*, vol. 22, no. 3, pp. 1070–1077, May 2007.

[7] R. J. Wai, C. Y. Lin, L. W. Liu, and Y. R. Chang, "High-efficiency single-stage bidirectional converter with multi-input power sources," *Proc. Inst. Elect. Eng.—Elect. Power Appl.*, vol. 1, no. 5, pp. 763–777, Sep. 2007.

[8] R. J. Wai, C. Y. Lin, and Y. R. Chang, "High step-up bidirectional isolated converter with two input power sources," *IEEE Trans. Ind. Electron.*, vol. 56, no. 7, pp. 2629–2643, Jul. 2009.

[9] H. Tao, J. L. Duarte, and M. A. M. Hendrix, "Three-port triple-half-bridge bidirectional converter with zero-voltage switching," *IEEE Trans. Power Electron.*, vol. 23, no. 2, pp. 782–792, Mar. 2008.

[10] H. Matsuo, W. Z. Lin, F. Kurokawa, T. Shigemizu, and N. Watanabe, "Characteristics of the multiple-input DC–DC converter," *IEEE Trans. Ind. Electron.*, vol. 51, no. 3, pp. 625–631, Jun. 2004.

[11] M. Marchesoni and C. Vacca, "New DC–DC converter for energy storage system interfacing in fuel cell hybrid electric vehicles," *IEEE Trans. Power Electron.*, vol. 22, no. 1, pp. 301–308, Jan. 2007.

[12] P. S. G. Giacomini, J. S. Scholtz, and M. Mezaroba, "Step-up/step-down DC–DC ZVS PWM converter with active clamping," *IEEE Trans. Ind. Electron.*, vol. 55, no. 10, pp. 3635–3643, Oct. 2008.

[13] J. Zhang, J. S. Lai, R. Y. Kim, and W. Yu, "High-power density design of a soft-switching high-power bidirectional DC–DC converter," *IEEE Trans. Power Electron.*, vol. 22, no. 4, pp. 1145–1153, Jul. 2007.

[14] L. P. Wong, Y. S. Lee, M. H. L. Chow, and D. K. W. Cheng, "A four-phase forward converter using an integrated transformer," *IEEE Trans. Ind. Electron.*, vol. 55, no. 2, pp. 817–831, Feb. 2008.

[15] N. Mohan, T. M. Undeland, and W. P. Robbins, *Power Electronics: Converters, Applications, and Design*. New York: Wiley, 1995.

[16] C. C. Chan, "The state of the art of electric, hybrid, and fuel cell vehicles," *Proc. IEEE*, vol. 95, no. 4, pp. 704–718, Apr. 2007.

[17] M. Ortuzar, J. Moreno, and J. Dixon, "Ultracapacitor-based auxiliary energy system for an electric vehicle: Implementation and evaluation," *IEEE Trans. Ind. Electron.*, vol. 54, no. 4, pp. 2147–2156, Aug. 2008.

[18] J. Bauman and M. Kazerani, "A comparative study of fuel-cell-battery, fuel-cell-ultracapacitor, and fuel-cell-battery-ultracapacitor vehicles," *IEEE Trans. Veh. Technol.*, vol. 57, no. 2, pp. 760–769, Mar. 2008.

Rong-Jong Wai (M'99–SM'05) was born in Tainan City, Taiwan, in 1974. He received the B.S. degree in electrical engineering and the Ph.D. degree in electronic engineering from Chung Yuan Christian University, Chung Li, Taiwan, in 1996 and 1999, respectively.

Since 1999, he has been with Yuan Ze University, Chung Li, where he is currently a Professor with the Department of Electrical Engineering, the Dean of the Office of General Affairs, the Chief of the Environmental Protection and Sanitation Office, and the Director of the Electric Control and System Engineering Laboratory. He is the author of a chapter in *Intelligent Adaptive Control: Industrial Applications in the Applied Computational Intelligence Set* (CRC Press, 1998) and the coauthor of *Drive and Intelligent Control of Ultrasonic Motor* (Tsang-Hai, 1999), *Electric Control* (Tsang-Hai, 2002), and *Fuel Cell: New Generation Energy* (Tsang-Hai, 2004). He has authored numerous published journal papers in the area of control system applications. His research interests include power electronics, motor servo drives, mechatronics, energy technology, and control theory applications.

Dr. Wai was the recipient of the Excellent Research Award in 2000 and the Wu Ta-You Medal and Young Researcher Award in 2003 from the National Science Council, Taiwan. In addition, he was the recipient of the Outstanding Research Award in 2003 and 2007 from the Yuan Ze University; the Excellent Young Electrical Engineering Award in 2004 and the Outstanding Electrical Engineering Professor Award in 2010 from the Chinese Electrical Engineering Society, Taiwan; the Outstanding Professor Award in 2004 and 2008 from the Far Eastern Y. Z. Hsu Science and Technology Memorial Foundation, Taiwan; the International Professional of the Year Award in 2005 from the International Biographical Centre, U.K.; the Young Automatic Control Engineering Award in 2005 from the Chinese Automatic Control Society, Taiwan; the Yuan-Ze Chair Professor Award in 2007 and 2010 from the Far Eastern Y. Z. Hsu Science and Technology Memorial Foundation, Taiwan; and the Electric Category Invent Silver Metal Award in 2007, the Electronic Category Invent Gold and Silver Metal Awards in 2008, the Most Environmental Friendly Award in 2008 from the International Invention Show and Technomart, Taipei, Taiwan; the University Industrial Economic Contribution Award in 2010 from the Ministry of Economic Affairs, Taiwan. His biography was listed in *Who's Who in Science and Engineering* (Marquis Who's Who) in 2004–2009, *Who's Who* (Marquis Who's Who) in 2004–2009, *Leading Scientists of the World* (International Biographical Centre) in 2005, *Who's Who in Asia* (Marquis Who's Who), *Who's Who of Emerging Leaders* (Marquis Who's Who) in 2006–2009, and *Asia/Pacific Who's Who* (Rifacimento International) in volumes VII and VIII.

Chung-You Lin was born in Pingtung City, Taiwan, in 1980. He received the B.S. and Ph.D. degrees in electrical engineering from Yuan Ze University, Chung Li, Taiwan, in 2004 and 2010, respectively.

Currently, he serves in the Army, Ministry of National Defense, Taipei, Taiwan. His research interests include resonant theory, power electronics, and renewable energy.

Jun-Jie Liaw was born in Yun-lin, Taiwan, in 1984. He received the B.S. degree in electronic engineering from Kun Shan University of Science and Technology, Tainan City, Taiwan, in 2006. He is currently working toward the Ph.D. degree in electrical engineering at Yuan Ze University, Chung Li, Taiwan.

His research interests include power electronics and IC design.

Yung-Ruei Chang (M'01) received the M.S. and Ph.D. degrees in electrical engineering from National Taiwan University, Taipei, Taiwan, in 1995 and 2004, respectively.

He is an Associate Researcher with the Institute of Nuclear Energy Research (INER), Atomic Energy Council, Longtan, Taiwan, where he has been working since 1996. From 2000 to 2004, he was with the technical transfer project of Taiwan's fourth nuclear power plant development, wherein he was involved in system reliability and fault-tolerant system design. He spent one year as a Visiting Engineer at STN ATLAS, Germany, and at General Electric, U.S., in 2000. Since 2005, he has been responsible for the power conditioning systems of the renewable energy project at INER. From June 2007 to September 2007, he was a Visiting Scholar at the Future Energy Electronics Center, Virginia Polytechnic Institute and State University, Blacksburg. His research interests include system reliability analysis, fault-tolerant systems, dependable computing, software reliability, power electronic systems, and renewable energy.